Journal of Structural Geology, Vol. 14, No. 3, pp. 343 to 359, 1992
Printed in Great Britain

0191-8141/92 $05.00+0.00

Development of wrench folds along the Border Ranges fault system, southern Alaska, U.S.A.

T. A. LITTLE*

Geology Department, Stanford University, Stanford, CA 94305, U.S.A.

(*Received* 7 *January* 1991; *accepted in revised form* 20 *August* 1991)

Abstract—En échelon folds in the central Chugach Mountains developed during Eocene brittle dextral-slip along the Border Ranges fault system. These wrench folds deformed an incompletely lithified alluvial fan complex as well as an adjacent phyllite belt. Wrench folding of phyllite was accommodated by flexural-slip between mechanical layers >1 m thick rather than by penetrative flexural-flow along the predominant cleavage.

The folds have non-cylindrical hinges that commonly deflect into subparallelism with, and are truncated by, adjacent strike-slip faults. Arrays of subsidiary faults and syntectonic veins indicate that fold hinges developed subparallel to the direction of maximum incremental elongation (λ_1), and that incremental λ_2 was vertical. The relationship between interlimb angle of these folds and the strike of their axial surfaces is consistent with variable clockwise rotation and tightening of these folds in a zone of heterogeneous, distributed wrench deformation. Early wrench folds trend clockwise of overprinting sets of more open folds, a relationship that suggests that the younger folds formed during the same progressive deformational event, but after the earlier set of folds had rotated clockwise, tightened and strain hardened. Megakinking attributed to strike-slip fault-bend folding resulted in local rotations of pre-existing folds. These results provide new insight into the geometry and kinematics of wrench folding, and do not support recent suggestions that the magnitude of shear stress on strike-slip faults is insufficient to induce wrench folding.

INTRODUCTION

THE TERM 'wrench folding' generally refers to folding caused by distributed simple shear deformation within, adjacent to, or above a zone of subvertical strike-slip faulting. Progressive development of folds in strike-slip fault zones has been investigated primarily by experimental deformation of analogue materials in laboratory shear-boxes (e.g. Cloos 1955, Tanner 1961, Ghosh 1966, Wilcox *et al.* 1973, Odonne & Vialon 1983, Naylor *et al.* 1986). Although natural examples of wrench folds have been described in the literature (e.g. Harding 1976, Sylvester & Smith 1976, Diblee 1977, Graham 1978, Moore 1979, Aydin & Page 1984, to name just a few), many are descriptions of two-dimensional fold trend patterns. Despite the potential for wrench folds to form hydrocarbon traps (e.g. Harding 1974) and a growing appreciation of the importance of strike-slip deformation within orogenic belts (e.g. Woodcock 1986), detailed field studies of natural examples are not common. A typical obstacle to studying wrench folds is a necessity to demonstrate that growth of the folds occurred as displacement was accumulating along adjacent strike-slip faults, rather than at some other time. Recently the basic notion that a belt of en échelon wrench folds develop by distributed simple shear in bedded sequences adjacent to basement strike-slip faults has been questioned. Mount & Suppe (1987) cite *in situ* stress and heat flow measurements along the modern San Andreas fault as evidence that there is a lack of significant shear stress resolved along that fault (see also comments by Harding 1988, Wickham 1988). Mount & Suppe (1987) and Namson & Davis (1988) argue that some of the classic examples of en échelon folds along the San Andreas fault may have been misinterpreted as wrench folds, thus raising some doubt about the applicability of the simple shear wrench folding model (e.g. Harding & Lowell 1979). Other workers have recently suggested that wrench folds are restricted to pure strike-slip or convergent strike-slip settings, and are not present where there has been a component of extension ('transtension') orthogonal to the mean strike of strike-slip faults (e.g. Harding *et al.* 1985).

Along a north-central part of the Chugach Mountains in southern Alaska, glaciated exposures of clastic sedimentary rocks and phyllite straddle the surface trace of the Border Ranges fault system, one of the major crustal boundaries in southern Alaska (Plafker *et al.* 1989) (Fig. 1). Rocks on both sides of the Border Ranges fault system (BRFS) are cut and dextrally offset within a braided system of steeply dipping faults, and have been deformed into a spectacular train of en échelon folds (Fig. 2). The age of both folding and strike-slip faulting can be demonstrated to be post-early Eocene and pre-early late Eocene (Little 1988, Little & Naeser 1989). In this paper I will interpret the development of en échelon folds, based on the results of 1:15,000 scale mapping and detailed structural studies of well-exposed rocks in this study area. I will argue that these folds developed obliquely to the strike of the BRFS in response to a component of simple shear distributed across a several kilometer wide zone along the BRFS. The data indicate that wrench folds nucleated over a wide range of initial orientations, probably due to variations in rheologic properties and strain within the geometrically complex BRFS. Fold hinges nucleated subparallel to the local direction of maximum incremental extension and locally

*Present address: Department of Geology, Victoria University of Wellington, P.O. Box 600, Wellington, New Zealand.

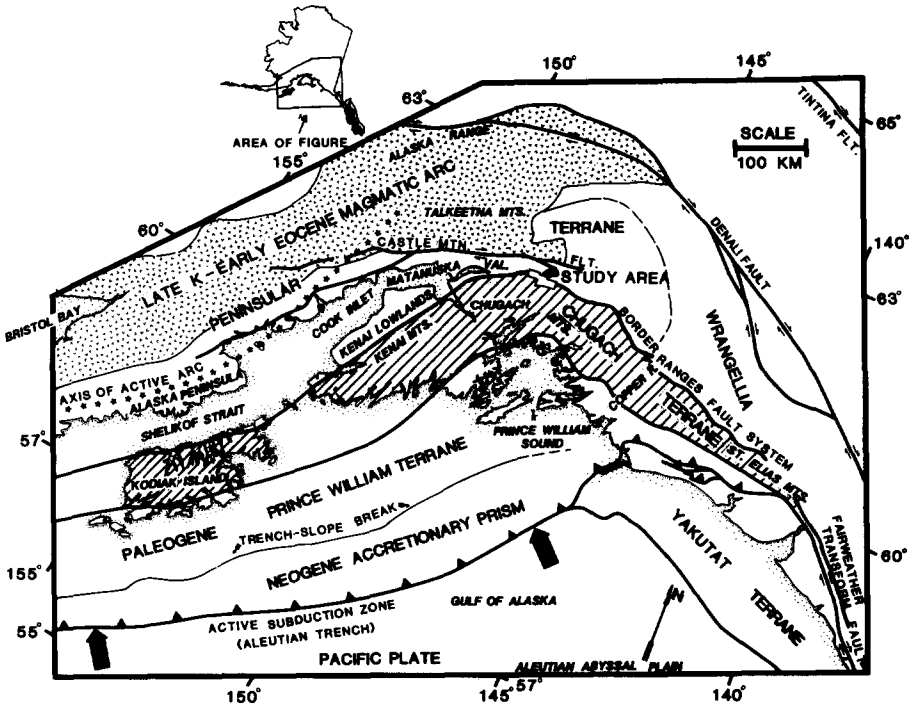

Fig. 1. Index map of a central part of southern Alaska showing tectonostratigraphic terranes (after Jones *et al.* 1981) and location of study area. Bold arrows show present-day relative motion of Pacific Plate with respect to North American Plate.

became increasingly more appressed as segments of their axial surfaces rotated clockwise towards subparallelism with the strike of faults in the BRFS. Later rigid body rotation of pre-existing wrench folds occurred when a relatively deformable fault block was folded around a right-stepping bend in a throughgoing strike-slip fault. Distributed deformation associated with a late-stage of oblique-slip faulting along the BRFS resulted in formation of a second generation of en échelon folds that were nucleated across older and more clockwise-rotated wrench folds.

GEOLOGIC SETTING

In the central Chugach Mountains, the BRFS forms the boundary between Mesozoic–Tertiary rocks of the Matanuska Valley–Cook Inlet basin on the Peninsular Terrane to the north and more intensely deformed Mesozoic rocks composing an accretionary prism to the south (Chugach Terrane). Metasedimentary rocks of the Chugach Terrane represent the deepest exposed levels of the subduction complex (Fig. 1). The McHugh Complex consists of ophiolitic rocks that have been dismembered into broken formation or melange (Fig. 3). The more outboard Valdez Group consists chiefly of turbidite sequences and hemipelagic rocks that were underplated to the base of the accretionary prism (e.g. Sample & Moore 1987). In early Cretaceous time the McHugh Complex was underthrust beneath the southern edge of the Peninsular Terrane (Pavlis 1982) along a system of thrust faults that are the oldest structural elements in the BRFS ('Border Ranges thrust system', Fig. 3, location A). The Peninsular Terrane embraces plutonic and volcanic rocks of a Jurassic island arc (e.g. Pavlis 1983, Burns 1985). Unconformably above the island arc sequence, rocks of the Matanuska Valley–Cook Inlet forearc basin consist of marine mudstones of the Cretaceous Matanuska Formation and fluvial–lacustrine rocks of the late Paleocene–early Eocene Chickaloon Formation (Fig. 3).

This paper concerns itself with en échelon folding that occurred during the last major deformation to affect this part of the BRFS, an Eocene event of dextral strike-slip deformation driven by rapid dextral-oblique convergence between southern Alaska and the oceanic Kula plate (e.g. Lonsdale 1988). In addition to folding, this deformation also included strike-slip fault-bend folding, local pull-apart graben development and dyke intrusion, much of which has been summarized elsewhere (Little 1990).

EOCENE WRENCH DEFORMATION EVENT

Timing constraints

Fossil leaves and spores both from the type Chickaloon Formation and from the study area are indicative of late Paleocene–early Eocene ages (J. A. Wolfe and H. M. Simpson personal communications 1985). Volcanic ash in the upper part of the Chickaloon Formation contain zircons with early Eocene fission-track ages of ~56–53 Ma (Triplehorn *et al.* 1984). In the Valdez Group, coarse muscovite growing in cleavage films of an *S*2 crenulation cleavage has yielded an early Eocene K/Ar age of ~57 Ma ± 1.7 Ma (1σ) (Little 1988). Thus the Chickaloon Formation was deposited at about the same

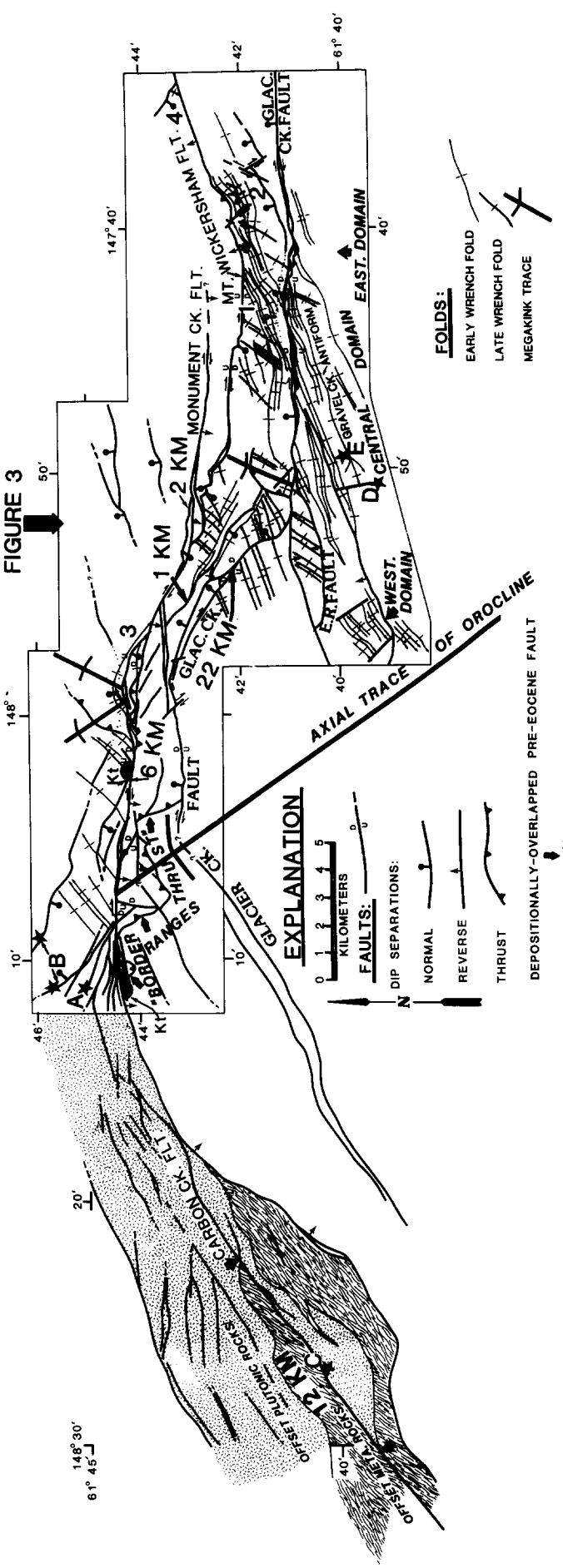

Fig. 2. Structural map showing fold and fault traces and senses of dip separation simplified from Burns *et al.* (1983), Little *et al.* (1986) and Little (1988). Dextral strike separations of offset map units (in kilometers) are shown adjacent to fault segments. Half-circles labeled 'Kt' schematically represent displaced parts of Cretaceous(?) trondhjemite stock. Numbers '1', '2', '3' and '4' refer to locations of fault-slickenline data presented in Fig. 7. Star-decorated letters 'A'–'E' indicate other locations mentioned in the text. Orocline axial trace inferred by connecting deflection in strike of BRFS with corresponding deflection of fault separating Chugach and Prince William terranes (see Fig. 1) farther south (Winkler & Plafker 1981).

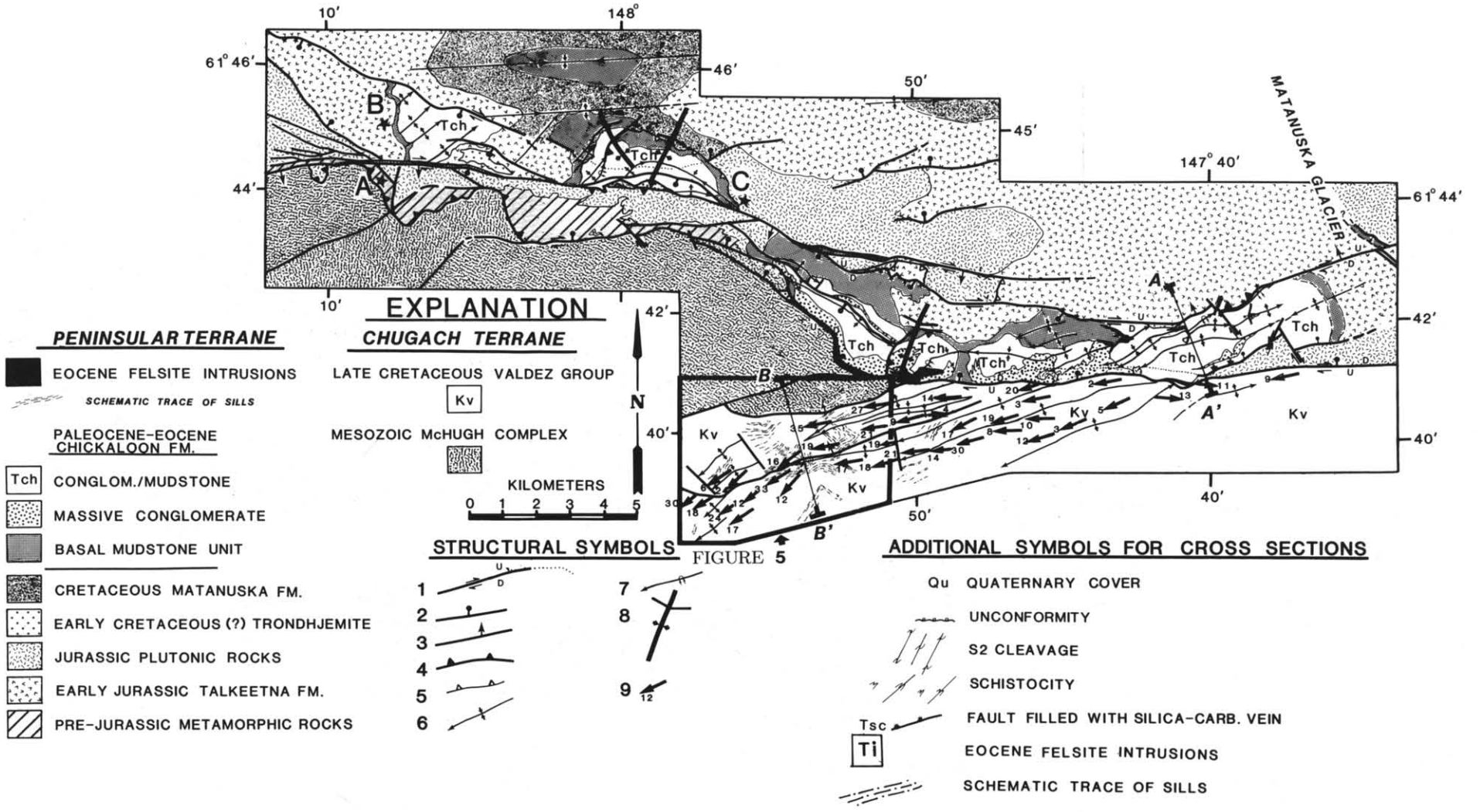

FIGURE 5

Fig. 3. Simplified geologic map of a central part of the northern Chugach Mountains after Burns *et al.* (1983), Little *et al.* (1986) and Little (1988). Star-decorated letters 'A', 'B' and 'C' refer to locations cited in text. Key to structural symbols: 1, fault; 2, normal-separation fault; 3, reverse separation fault; 4, thrust fault; 5, décollement fault; 6, axial trace of wrench fold; 7, axial trace of overturned fold; 8, axial trace of fault-bend megakink; 9, mean trend and plunge of L_2 lineation in the Valdez Group (averages of 10–40 measurements in selected domains).

time as the Valdez Group was being metamorphosed, yet the two units are now juxtaposed across the Glacier Creek fault (Figs. 2 and 3).

Undeformed post-tectonic felsic dykes intrude most throughgoing faults in the BRFS, including the Glacier Creek fault (Little & Naeser 1989). Three zircon fission-track ages on the dykes range (with 1σ errors) from 41.3 ± 3 Ma to 47.8 ± 4 Ma (*ibid.*). One of the dated dykes is a sill-like body intruded into a fold culmination in the Chickaloon Formation; other dykes cross-cut faults that in turn cut folds (Little 1988). Together these age constraints thus indicate a post-early Eocene and pre-early late Eocene age for both dextral-slip faulting and en échelon folding along this part of the BRFS.

Strike-slip faulting

Eocene faults in the central part of the BRFS comprise a braided network of generally E-striking and steeply dipping faults. In addition to the predominant set of E-striking faults, inferred *R*-shears (e.g. Naylor *et al.* 1986) and en échelon normal faults occur as discontinuous subsidiary faults (e.g. locations A and B, Fig. 2). The throughgoing Glacier Creek fault dips moderately north to vertical, has gently E-pitching slickenlines and makes a sharp right-stepping bend in a central part of the study area, where a small pull-apart graben is developed (Figs. 2 and 3).

Determination of the total amount of dextral-slip across the BRFS during this Eocene event is hindered by juxtaposition of differing structural levels across the present-day BRFS (deeper to the south) and a paucity of marker horizons or piercing points that can be correlated across the fault system. A summary of inferred strike separations along mapped faults is given on Fig. 2 and Table 1, and suggests a minimum cumulative displacement of 34 km.

These Tertiary faults are brittle structures at the present levels of exposure, and most crop out as slickensided surfaces with horizontal or gently plunging striae. The Glacier Creek fault is filled by a several m-thick vein of chlorite–quartz–dolomite rock and an undeformed Eocene felsite dyke. Emplacement of the multiply-brecciated and partly mylonitic vein (Little & Naeser 1989) was probably triggered by dilational earthquake ruptures leading to hydraulic pumping of fluids into the rupture zone (Sibson 1987).

Nature of the Chickaloon Formation during folding

Lithofacies studies indicate that the Chickaloon Formation was deposited syntectonically along the BRFS as an alluvial fan complex controlled by down-to-the-north displacement along basement faults (e.g. Fig. 4, A–A′). Where it abuts the Glacier Creek fault, the Chickaloon Formation consists of a thick wedge of conglomerate derived locally from the Chugach Terrane. An abundance of thick mudstone and local coal beds interbedded with conglomerate in that formation suggests rapid subsidence of the fault-controlled basin in which the alluvial fan complex was deposited (Little 1988).

The Chickaloon Formation is metamorphosed in the albite–laumontite zone of the zeolite facies. Mean vitri-

Table 1. Synopsis of Tertiary deformation events along a central part of the Border Ranges fault system

First-phase wrench structures		Later-phase transtensive structures	
Folds	Faults/veins		
Chickaloon Formation			
F_1 **folds.** Regional upright en échelon set with NE–SW-trending subhorizontal axes. Typically doubly plunging chevron folds with sigmoidal axial traces. $\lambda/2$ = 50–300 m (mean ~150). Class 1b (congom./ss./mudst.) or Class 3 (some muds. bed). No axial surface cleavage. Decoupled along subhorizontal décollements and basal unconformity.	**Dextral slip faults.** East-striking Glacier Ck. fault (22 km). Carbon Ck. fault (~12 km). Mt. Wickersham fault (? km), cut by younger Monument Ck. fault (2 km max.). Numerous discontinuous **Riedel (R) shears** and local **conjugate strike-slip faults.** Discontinuous **normal faults** transverse to F_1 axial traces and **thrust faults** subparallel to axial traces.	F_{2a} **folds.** Found only in pull apart graben along oblique segment of Glacier Ck. fault. Upright set with ENE–WSW-trending gently to moderately plunging axes.	F_{2b} **folds.** Regional set, best developed in eastern part of study area. Also affect McHugh Complex. Upright set with NNE–SSW-trending gently to moderately plunging axes. Sinusoidal or concentric with rounded hinges. Laterally discontinuous; markedly non-cylindrical where superposed across F_1 axial traces. $\lambda/2$ = 50 m–3 km. Open to tight. No axial surface cleavage. **Normal or oblique normal faults** transverse to F_2 axial traces. **Eocene felsic dykes** and **quartz dolomite vein** emplaced along Glacier Ck. fault: interpreted as dilational features syntectonic with F_{2b}.
Valdez Group			
F_4 **folds.** Regional upright en échelon set with NE–SW-trending subhorizontal axes. Typically doubly plunging chevron or box folds with sigmoidal axial traces. $\lambda/2$ = 50–800 m (mean ~300 m). Class 1b parallel folds. No axial surface cleavage. Probably cogenetic with F_1 in Chickaloon Formation.	Fold trains compartmentalized by transverse **displacement transfer faults.** **Reverse oblique faults** subparallel to axial traces. Fibrous quartz **extension gashes** subparallel to fold profile plane.		F_5 **folds.** Regional set, best developed in eastern part of study area. Upright set with NNE–SSW-trending gently to moderately plunging axes. Disharmonic with sinusoidal, chevron, or box shaped profiles. Strongly non-cylindrical. $\lambda/2$ = 10 cm–8 m. Open to close. No axial surface cleavage. Probably cogenetic with F_{2b} in Chickaloon Formation.

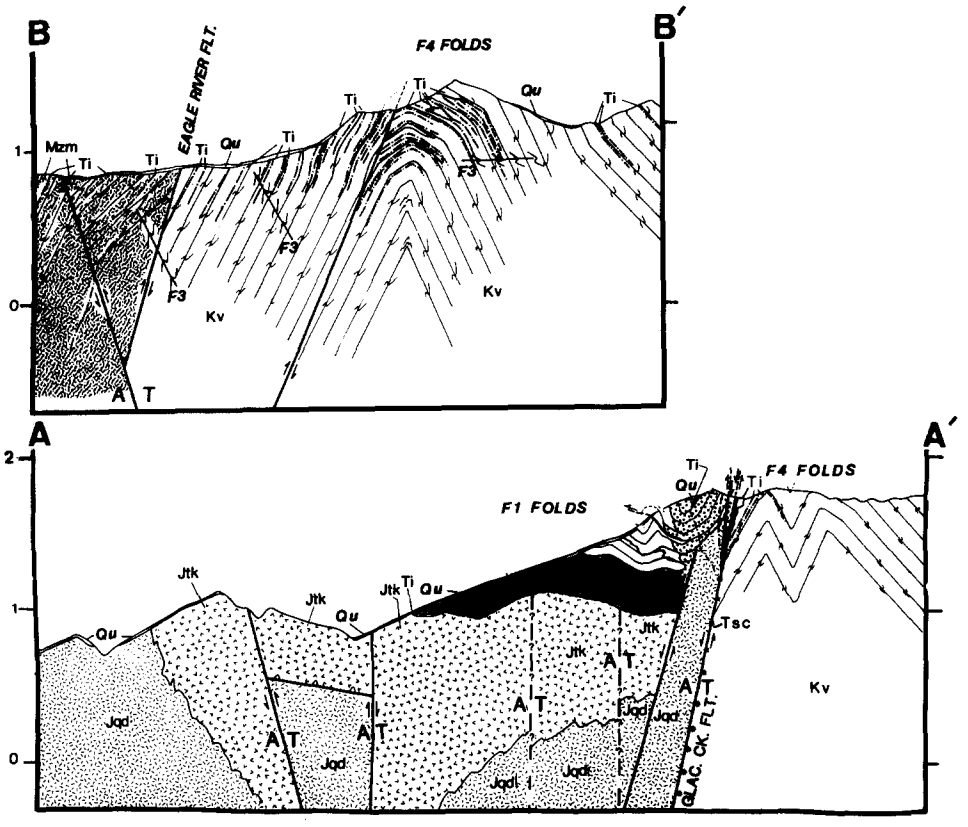

Fig. 4. Structural cross-sections. Elevations in km above sea level. No vertical exaggeration. Location of sections shown in Figs. 3 and 5. See Fig. 3 for explanation of symbols.

nite reflectance values (R_0) in the Chickaloon Formation increase with stratigraphic depth from ~0.5 to a maximum mean value of ~1.1 at the base, suggesting that presently exposed rocks in the Chickaloon Formation had been heated to a maximum temperature of ~100–175°C prior to folding (Little 1988). Apatite fission-track data indicate that these rocks did not cool to below ~100°C until early Miocene time (Little & Naeser 1989). Using the present geothermal gradient of ~20–25°C km^{-1} in the Cook Inlet basin (Magoon 1986), the fission-track data suggest a minimum of 4 km of erosion of rocks originally overlying the Chickaloon Formation to account for this cooling.

Despite the above evidence for moderate heating and burial, there is little evidence for intragranular deformation in strongly deformed rocks of the Chickaloon Formation. Even where mudstone is tectonically thickened in the hinges of close folds, a cleavage is not present, and zones of tectonic breccia or cataclastic rocks are absent from conglomerate adjacent to throughgoing faults.

The available geochronology indicates an ~8 m.y. maximum time interval between early Eocene (~56 Ma) deposition of upper parts of the Chickaloon Formation and Eocene folding of those rocks (~48 Ma, intrusion of post-tectonic dykes). The apparent brevity of this span accords with the above inferences that the Chickaloon Formation may have been a rapidly deposited, incompletely lithified sequence that deformed largely by particulate flow during its Eocene deformation.

PROGRESSIVE FOLDING HISTORY

Introduction

Over 8000 measurements of planar and linear mesoscopic structural elements were recorded during study of the en échelon foldbelt, and the area was divided into over 130 structural domains that coincide with planar limb regions of individual folds or their narrow axial regions. Wherever possible, orientation data were used to define the local orientation of individual fold hinges, and the mean orientation of fold limbs (e.g. Fig. 5, data sets E, F and G). Mean fold hinge and limb orientations were determined by computer using the eigenvector technique of Woodstock (1977). The number of measurements of planar data which were used to determine mean hinge or limb orientation for a given domain varied between 11 and 169. Most domains contained at least 40 measurements of the folded surface (bedding in the Chickaloon Formation, S_2 in the Valdez Group). Because of the steep topography in this part of the Chugach Mountains (commonly about 1 km of local relief), mapped axial traces generally make an angle of 10° or more with respect to the associated fold hinge. Together these two lineations could thus be used to provide a reliable estimate on the local orientation of fold axial surfaces. The raw data for this analysis and accompanying geologic map are presented in Little (1988). A synopsis of salient geometric features of these en échelon folds is presented in Table 1.

Superposed folding in the Chickaloon Formation

Most of the Chickaloon Formation consists of units of conglomerate and sandstone, up to 2 m thick, that are overlain by subordinate mudstone. These rhythmically bedded rocks are preserved in a 3–4 km wide fault slice down-dropped along the northern side of the Glacier Creek fault (Fig. 3). The Chickaloon Formation has been deformed into map-scale en échelon folds (F_1) that have gently NE- or SW-plunging axes and upright or steeply dipping axial surfaces (Fig. 2) (Little 1990, fig. 7a). This belt of en échelon folding is aerially restricted to the BRFS along the northern flank of the Chugach Mountains. Less densely faulted rocks in the adjacent Matanuska Valley are folded about ENE-trending, gently plunging axes that are subparallel to the mean trend of the forearc basin (northwest edge of Fig. 3). Folding in the Matanuska Valley occurred in middle Eocene–late Oligocene time (Bruhn & Pavlis 1981), and thus was at least in part younger than Eocene folding in the Chugach Mountains.

In profile, F_1 folds in the Chickaloon Formation are sinusoidal in shape at open interlimb angles and amplitudes, and chevron-shaped where more tightly appressed. This variation may represent snapshots of different stages in their developmental sequence (e.g. Reches & Johnson 1976), although some chevron folds become broadly rounded with depth as their axial surfaces approach the basal décollement. Most folds have planar or gently curved limbs and a narrow, angular to rounded hinge region. Interlimb angles range from about 120° in the lowest amplitude folds to about 40° in the tightest folds. Bedding-subparallel décollements locally separate fold trains that are out of phase with respect to each other, particularly in mudstone-rich sequences (e.g. Little 1990, fig. 6). Where the base of the Chickaloon Formation is exposed (Fig. 3, locations B and C), beds are in low-angle fault contact against the underlying basement of Jurassic igneous rocks. This décollement probably underlies most or all of the fold belt. One or more steeply dipping strike-slip faults may underlie this décollement, controlling development of en échelon fold sets in superjacent rocks of the Chickaloon Formation (e.g. Fig. 4, A–A′).

F_1 folds have non-planar axial surfaces and undulatory hinges that commonly terminate laterally against faults. A thrust-fault cuts out the mutual limb of some anticline–syncline pairs (e.g. Fig. 4, A–A′). Axial traces are commonly sigmoidal in plan, deflecting at their northeastern and southwestern tips into subparallelism with bounding strike-slip faults (Fig. 2). Most folds are doubly-plunging, and the ends of anticlines typically plunge into bounding strike-slip faults. In a few cases, a culmination is developed immediately adjacent to bounding faults (e.g. Little 1990, fig. 4). The culminations probably coincide with zones of increased finite layer-parallel shortening, and are interpreted to mark sites of fold nucleation away from which the fold hinges propagated laterally (e.g. Ramsay 1967, Harding 1976, Dubey & Cobbold 1977, Bamford & Ford 1990).

F_2 sets of en échelon folds can be recognized because their variably plunging hinges are overprinted across pre-existing F_1 fold limbs (Fig. 2) (see also Little 1990, fig. 4). On the basis of orientation and location, an F_{2a} set of post-F_1 folds that have axial surfaces that strike ENE can be differentiated from an F_{2b} set having upright axial surfaces that strike NNE (Little 1990, figs. 8a & b). Both sets of F_2 folds are broad parallel folds with sinusoidal or concentric profiles, rounded axial regions, and open interlimb angles, although locally tight folds are present.

Superposed folding in the Valdez Group

In the study area, the Valdez Group consists chiefly of pelitic phyllite. The dominant cleavage, S_2, is deformed into a series of km-scale folds that have an en échelon disposition with respect to the BRFS. These F_4 folds, which post-date an F_3 generation of local mesoscopic folds, have axes that plunge gently to the northeast or southwest, and have steeply dipping axial surfaces.

Most F_4 folds in the Valdez Group are chevron-shaped. Some chevron folds pass upward into a box-fold having a gently rounded 'top' (Fig. 2, location E, and Fig. 4, B–B′). These broad axial regions are commonly zones of pervasive mesoscopic folding. Like F_1 folds in the Chickaloon Formation, F_4 folds in the Valdez Group do not have an axial planar cleavage, except for rare spaced crenulations. Mesoscopic F_4 folds commonly have mean axial directions that are not parallel to the larger order folds upon which they occur (Little 1990, fig. 7d). Interlimb angles of F_4 folds range from 40° to 130° but most fall in the range of 50–90°, and a segment of one fold has an interlimb angle of ~25°.

F_4 folds are commonly sigmoidal in plan and terminate by fault truncation or die out laterally. The best examples of S-shaped deflections are provided by the Gravel Creek antiform, whose axial surface makes several sigmoidal bends (Fig. 2). Where the eastern end of that fold is deflected into subparallelism with the adjacent Glacier Creek fault, a doubly-plunging culmination is developed in the fold (Little 1990, fig. 4). Similar deflections and culminations occur where other F_4 folds abut the Glacier Creek fault, a geometry reminiscent of F_1 folds in the Chickaloon Formation. Some folds die out where two adjacent axial surfaces converge (Fig. 5, location B). Other folds terminate against transverse structures that are probably displacement transfer faults (e.g. Fig. 2, location D). Analogous structures have been observed in experimental models by Dubey & Cobbold (1977), who attribute such high-angle faulting to interference between laterally propagating fold trains that are out of phase with respect to each other.

An F_5 generation of folds deforming S_2 in the Valdez Group are restricted to a 1–2 km wide belt along and to the south of the Glacier Creek fault in the eastern part of the study area. In orientation these folds resemble F_{2b} folds in the Chickaloon Formation (Little 1990, fig. 8c). F_5 folds are strongly disharmonic folds that vary from rounded to angular to box-shaped.

Chevron folding of phyllite in the Valdez Group was accommodated by flexural-slip between >1 m thick mechanical layers rather than by penetrative flexural-flow along the predominant cleavage. Local dilation resulting from flexural-slip along m-thick layers is indicated by the presence in the axial regions of F_4 folds of open triangular saddle reefs, in some cases, filled with quartz. The axial surfaces of mesoscopic F_3 folds deformed across larger F_4 chevron folds (Fig. 4, B–B′) can be restored to a common 'pre-F_4' attitude simply by rotating them together with the chevron fold limbs about the local F_4 hinge direction. In Fig. 5, F_3 data in stereonets C and D are shown 'unfolded' in corresponding nets C′ and D′. This observation suggests that F_3 axial surfaces were rotated on the limbs of F_4 chevron folds without appreciable rotation of opposite sense resulting from flexural-flow within the chevron fold limbs (e.g. Ramsay 1967). F_4 chevron folds thus developed by flexural-slip between layers that were thicker than the <10–50 cm amplitude of the F_3 folds. Similarly, Tanner (1989) described chevron folds in which flexural-slip occurred along widely spaced mechanical layers. Micro-

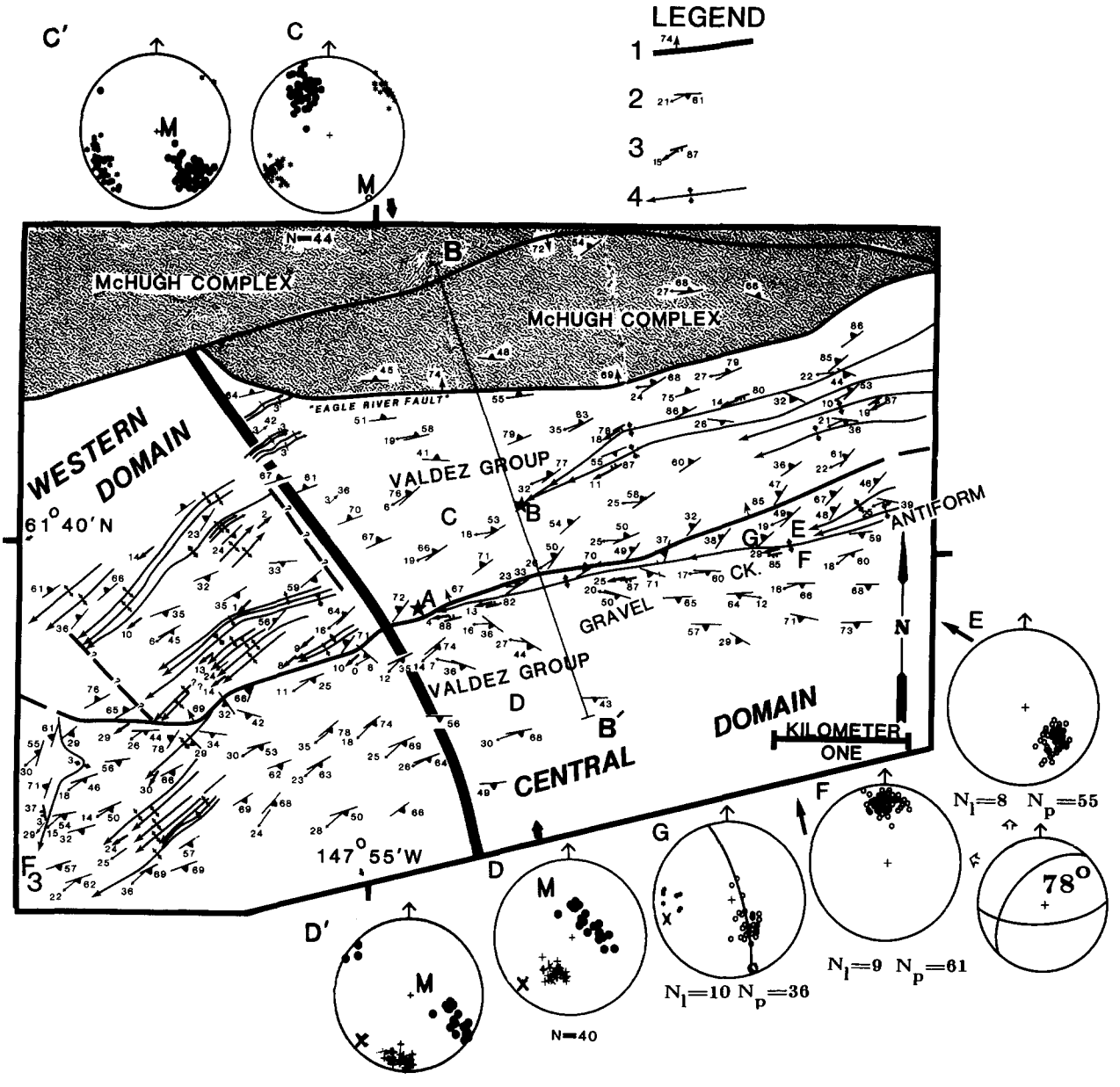

Fig. 5. Simplified geologic map of a western part of the study area with structural data for selected domains. Location of map shown in Fig. 3. Heavy line is boundary between central and western domains. Key to structural symbols in legend: 1, fault, showing dip; 2, attitude of S_2 cleavage, and trend of crenulation lineation, L_2; 3, attitude of fold axial surface and hinge; 4, axial trace of fold. Star-decorated letters 'A' and 'B' refer to locations mentioned in the text. Lower-hemisphere equal-area projections 'C' and 'D' show present-day attitudes of mesoscopic F_3 folds measured on northern and southern limbs, respectively, of the Gravel Creek antiform, whereas C′ and D′ show the same data after being rigidly 'unfolded' about the hinge of that F_4 fold. In these projections, 'M' indicates the pole to mean S_2 in a domain (shown restored to subhorizontal attitude in C′ and D′); plus-marks are hinges of F_3 folds; filled circles, poles to F_3 axial surfaces; and 'X', mean F_4 hinges. Projections for locations 'E' and 'F' show mean attitudes of northern and southern limbs of part of the Gravel Creek antiform (inset shows calculated interlimb angle) and 'G' shows data from part of the axial region of that fold. In 'G', small open circles are poles to the S_2 cleavage; and asterisks, L_2 crenulation lineations.

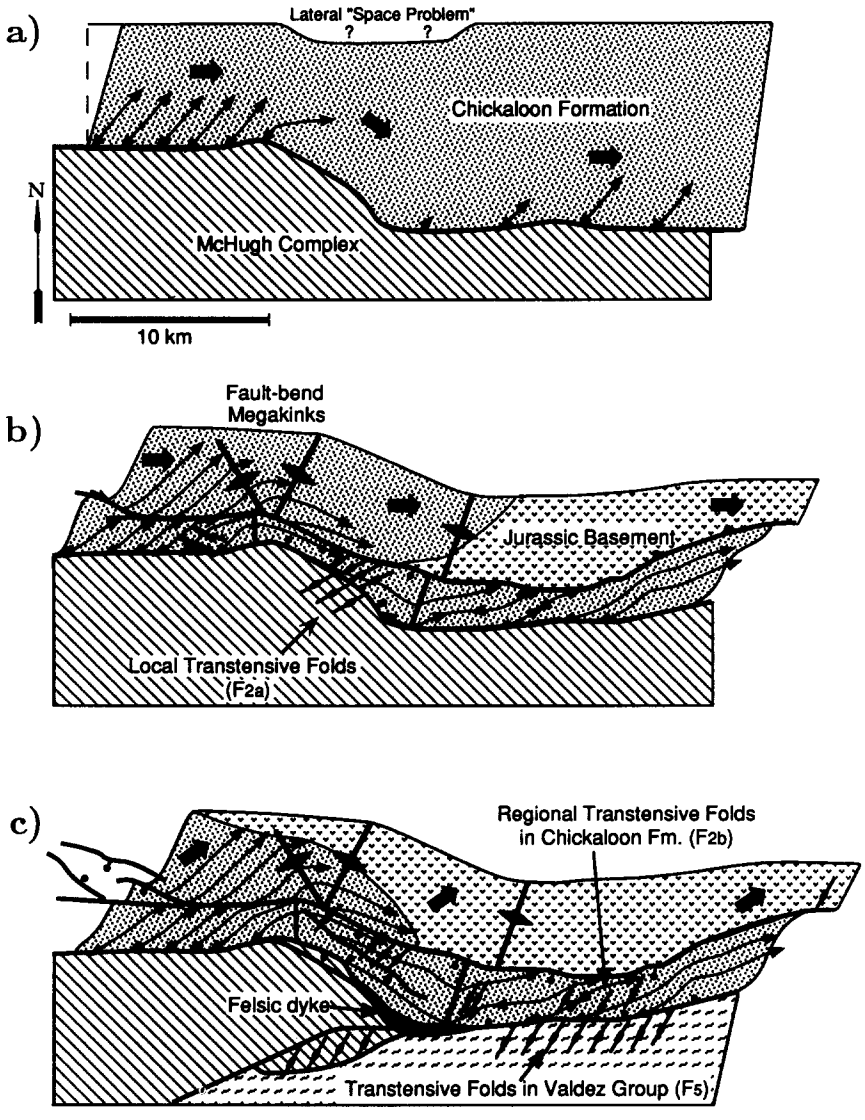

Fig. 6. Interpretive diagram illustrating Eocene development of wrench structures along a central part of the BRFS. For simplicity, late-stage displacement along Monument Creek fault has been undone. Heavy arrows show relative displacement of northern vs 'fixed' southern fault blocks. (a) Nucleation of wrench folds at ~45° to Glacier Creek fault and beginning of dextral-slip faulting and fault-bend folding of Chickaloon Formation as it is translated around right-stepping bend. (b) Later configuration after completion of fault-bend folding and during early stages of pull-apart graben development. Note superposition of late-stage 'transtensive' F_{2a} folds locally in pull-apart graben across clockwise-rotated F_1 wrench folds. (c) Configuration during late stage of oblique-normal faulting, dyke intrusion and distributed transtensive deformation along the BRFS. Normal-separation along Glacier Creek fault uplifts Valdez Group and results in erosion of overlying McHugh Complex.

structural observations led Nakahara & Wiltschko (1986) to conclude that the angular hinge region of a chevron folded quartzite bed was brittlely deformed, whereas the planar limbs of the fold were largely undeformed and had been passively rotated. A similar style of deformation may have prevailed during chevron folding of phyllite in the Valdez Group.

LATE-STAGE MEGAKINKS AND A PULL-APART GRABEN

In the central part of the study area F_1 folds in the Chickaloon Formation have been rotated clockwise between two sets of steeply plunging megakink boundaries (Fig. 2). Within this ~9 km wide kink band, F_1 folds retain their en échelon disposition with respect to the Glacier Creek fault, but their rotated hinges trend SE (Little 1990). These megakinks have been interpreted as strike-slip fault-bend folds forming during 22 km or more of dextral-slip translation of a relatively deformable northern block across a competent strike-slip ramp to the south (Little 1990). Figures 6(a) & (b) illustrate my interpretation of the fault-bend folding event.

As mentioned above, F_2 folds within the kink-band region (F_{2a} set) trend ENE, whereas elsewhere such late-stage folds trend NNE (F_{2b} set). The unique orientation of F_{2a} folds may have resulted from clockwise rotation of the folds as they were translated into the kink band from a nucleation site farther west. Alternatively, such folds may have formed essentially *in situ* as a result of a distributed transtensive deformation within the pull-

apart graben (e.g. Sanderson & Marchini 1984, fig. 11). The pull-apart graben is defined by several NW-striking fault splays with normal-separation, including the NW-striking segment of the Glacier Creek fault (Fig. 2). As it enters the pull-apart, a felsic dyke intruding the Glacier Creek fault abruptly widens from its average width of 2–3 m to over 250 m, suggesting that the middle or late Eocene age dyke (47.8 ± 4 Ma, apatite fission-track age, Little & Naeser 1989) was emplaced along a dilational jog in the Glacier Creek fault. An interpretation of the kinematic development of late-stage folds and the graben is presented in Figs. 6(b) & (c).

RELATIONSHIP OF FOLDING TO INCREMENTAL STRAIN AND STRESS

Mesoscopic scale incremental structures associated with the above described en échelon folds are consistent with development of the folds in a zone of distributed wrench deformation. Below I briefly describe arrays of minor faults, folds and veins which are indicative of the stress–strain states prevailing during development of these folds, and which also provide some insight into the way in which progressive bulk rotational strain was accommodated during folding of rocks in the BRFS.

Evidence for axial elongation of folds

Minor faults and veins in folded rocks of the study area suggest that the local direction of maximum incremental stretch (λ_1) was subparallel to the hinge lines of en échelon folds, a relationship that is consistent with deformation by a wrench style of simple shear. In the eastern part of the study area, F_1 folds in the Chickaloon Formation are locally offset by conjugate sets of strike-slip faults that are symmetrically disposed with respect to fold hinges and have resulted in an axial elongation of the folds (Fig. 2, location 2). Dubey (1980) described a similar relationship between folds and conjugate vertical faults in a model experiment where the intermediate strain axis (λ_2) was vertical and the direction of maximum incremental and finite elongation (λ_1) was parallel to the fold hinges. In the same area, F_1 folds in the Chickaloon Formation are also locally cut by conjugate sets of normal faults that strike traverse to the axial trace. Similarly, a common feature of F_2 folds, especially those with close or tight interlimb angles, is their lateral truncation by transverse normal faults, a deformation resulting in extension of the fold subparallel to their axial traces (e.g. Fig. 2, location 4). Minor axial elongation of F_4 folds in the Valdez Group is accommodated by mesoscopic tension gashes, oriented orthogonal to the hinges of adjacent F_4 chevron folds, that are filled with fibrous quartz (Little 1990, plate 2). Rather than reflecting hinge-parallel extension of regional nature, however, it is also possible that such extensional veins could result from a localized strain during propagation of non-cylindrical fold hinges (e.g. Dubey & Cobbold 1977).

Inversions for mean deviatoric stress tensor

Numerical techniques for inversion of the relative deviatoric stress tensor from fault-slickenline data can be useful tools for interpreting deformation at brittle levels of the crust (e.g. Angelier 1984). These methods assume that each sampled fault plane slipped independently in a direction parallel to its resolved shear stress, that each of these slip events was governed by some homogeneous deviatoric stress tensor, and that there has been no differential, post-faulting rotation between sites. By use of a linear least-squares technique, the method of Michael (1984) solves for a best-fit tensor that yields similar magnitudes of resolved shear traction on each plane. For Coulomb faulting at moderate depths, similar magnitudes of resolved shear stress is a reasonable approximation because friction on failure planes is controlled chiefly by the hydrostatic part of the stress tensor (Michael 1984).

Stress tensors were inverted using Michael's (1984) program from sets of 18–28 mesoscopic faults measured at four different locations in folded sequences of thick-bedded sandstone and conglomerate in the Chickaloon Formation. Three of the sites were located on the limb or axial region of an F_1 fold (Fig. 2, locations 1, 2 and 3), and a fourth one in the axial region of an isoclinal F_2 fold (location 4). Sense of slip on faults was determined by offset bedding surfaces and fibrous calcite slickenfibers. Measured displacements on the faults varied between 0.5 and 30 cm.

The solutions are consistent with a wrench style of deviatoric stress in which σ_2 was subvertical and σ_3 was subparallel to adjacent fold hinges. Data sets from locations 1 and 2 are dominated by sets of NNE- and NW-striking strike-slip faults and by lesser SW-dipping oblique-slip faults (Figs. 7a & c). The corresponding stress tensor solutions (Figs. 7b & d) indicate that σ_2 was subvertical and that σ_3 was subparallel to adjacent gently plunging F_1 fold hinges. The data and best-fit stress tensor for location 3 are similar, but both F_1 fold hinges and inferred principal stress directions have apparently been rotated clockwise ~60–70° about a vertical axis. This rotation is a result of deformation of rocks north of the curved Glacier Creek fault within the kink band. Location 4 is in the axial region of a tight fold interpreted on the basis of its orientation to be an F_2 fold. The upright axial surface of this fold is transverse to a normal fault truncating the fold, and approximately contains the slickenline lineation on that fault (Fig. 7g), a relationship indicative of brittle elongation of the fold, possibly after the tightly appressed fold had 'locked up'. Note that the best-fit σ_3 direction is subparallel to the adjacent fold hinge and that σ_2 is subvertical, similar to the relationships described above for faults in regions of F_1 folding.

Given the many assumptions implicit in stress tensor inversions for such folded (and thus variably rotated) strata, and the marked heterogeneity of stress expectable in folds (e.g. Donath & Parker 1964), the results from these four sites yield remarkably similar results. In

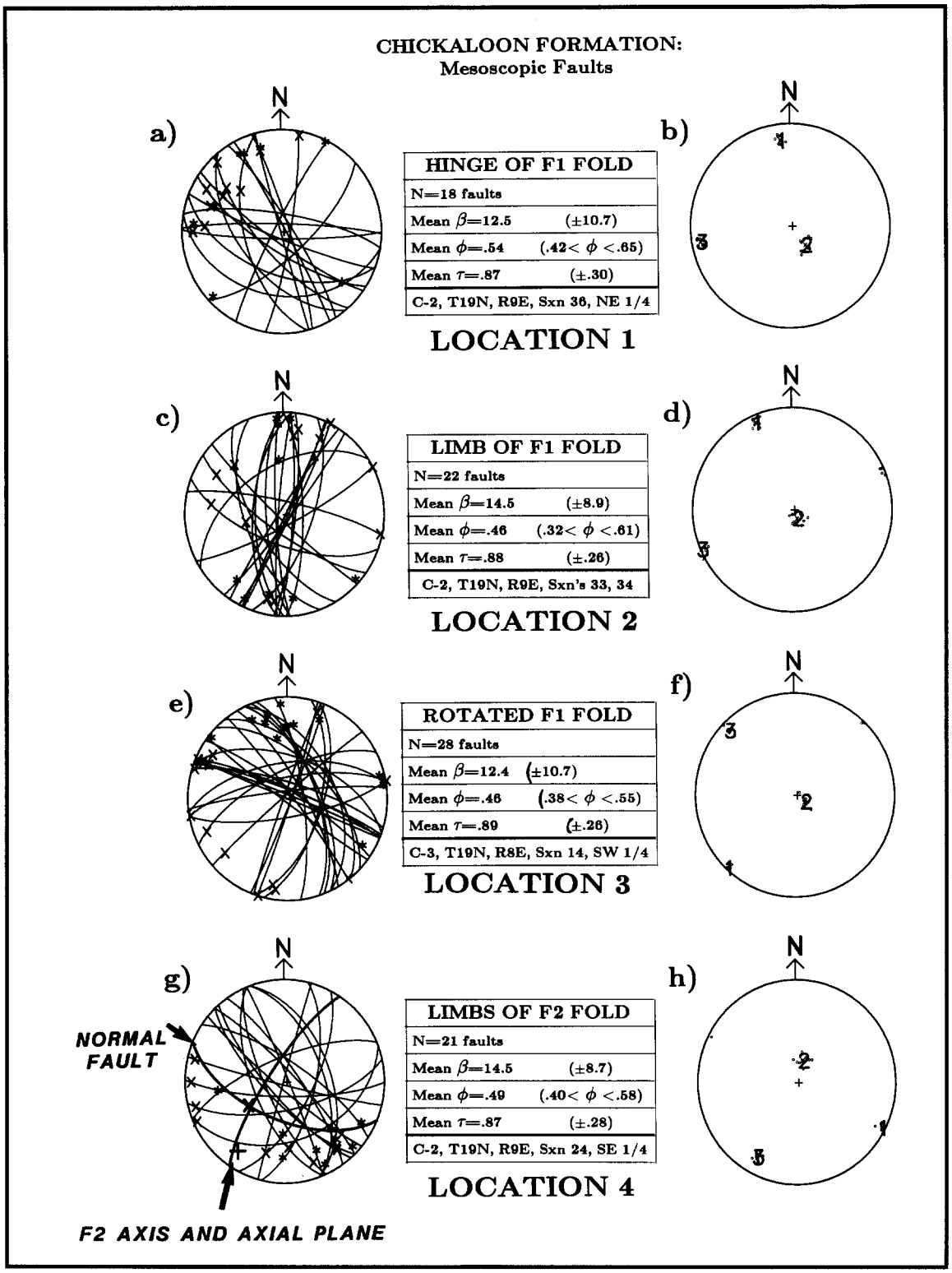

Fig. 7. Mesoscopic fault-slickenline data (on left) and corresponding best-fit deviatoric stress tensor (on right) determined by computer inversion technique of Michael (1984). Locations of sampled populations 1–4 are shown on Fig. 2. For a given fault, β, is the angular deviation between the measured slickenline and theoretical shear stress vector predicted by the best-fit stress tensor solution. The value, λ, is mean magnitude of resolved shear stress in a given data set and is a measure of the success of the linear least squares inversion in achieving a normalized shear stress magnitude of unity on each fault plane. The parameter, ϕ ($0 \leq \phi \leq 1$), is a measure of the shape of the best-fit deviatoric stress ellipsoid [$\phi = (\sigma_2 - \sigma_3)/(\sigma_1 - \sigma_3)$]. Mean ϕ values between 0.45 and 0.55 are consistent with approximate plane stress conditions. On data plots (a, c, e, g), great circles denote fault orientations on lower-hemisphere equal-area projections. Measured slip-vectors on these faults are defined with respect to a 'fixed' footwall. Striations indicated by asterisk (*) denote slip vectors that intersect the upper hemisphere (i.e. hangingwall-up motion) whereas those indicated by X represent slip vectors that intersect the lower hemisphere (hangingwall-down). In the solutions (b, d, f, h), numbers '1', '2' and '3' denote best-fit directions of most, intermediate and least principal compressive stress. Small open circles are other possible orientations of these eigenvectors determined by sampling within the 95% confidence interval around the variance–covariance error ellipsoid for stress tensor elements. In stereonet (g) for location 4, heavy great circles represent axial plane of tight F_2 fold in the Chickaloon Formation and a normal fault that truncates that fold (the large X shows measured slickenline on that normal fault).

each case σ_2 is determined to be subvertical and σ_3 subparallel to the local orientation of fold hinges. Apparently mesoscopic faulting post-dated the folding, or possibly occurred during the latest stages of folding, so that mesoscopic fault arrays were superposed across already rotated strata. My interpretation is that the observed brittle overprint was a response to strain hardening of progressively tightened and increasingly dewatered(?) folds. The orientation of the least compressive stress, σ_3, being subparallel to en échelon fold hinges reinforces previously described evidence for axial elongation of the folds and is consistent with development of the folds in a wrench shear zone.

Obliquity of principal stress and strain axes to strike of adjacent faults

Minor structures and inversions for the stress tensor suggest that en échelon folds in the BRFS were extended axially, and that incremental λ_2 and σ_2 were vertical during their development. The observation that F_1 folds in the Chickaloon Formation trend clockwise of younger and generally less tightly appressed F_2 folds suggests the progressive development of these fold sets in a zone of distributed dextral wrench deformation. In a similar way, F_4 folds in the Valdez Group trend in clockwise direction with respect to overprinting F_5 folds. Large F_4 folds also commonly trend clockwise of younger(?) mesoscopic F_4 folds in their hinges. Superposition of younger sets of folds upon apparently more clockwise-rotated, older en échelon folds suggests a progressive deformational event involving a rotational bulk strain path associated with dextral shearing. According to this model, later sets of folds formed after pre-existing sets had rotated clockwise, tightened and strain hardened, with the hinges of the younger folds nucleating subparallel to a direction of maximum incremental stretching that was markedly oblique to adjacent faults.

For the case of progressive simple shear deformation, fold axes should trend at no more than 45° to the shear zone boundaries. The observed ~62° angle which the mean strike of F_{2b} axial surfaces make with respect to E–W-striking throughgoing faults in the BRFS suggests that the younger folds developed when distributed deformation across the BRFS shear zone had become slightly transtensive (Sanderson & Marchini 1984) (Fig. 6c). This interpretation is consistent with the normal dip-separation across the Glacier Creek fault, intrusion of that fault zone by Eocene dykes, and emplacement of dilational veins along that fault. In a wrench zone that undergoes a late increment of transtensive deformation, the direction of maximum finite contraction (λ_3) is disposed more nearly parallel to the shear zone boundaries than for the case of ideal simple shear. This relationship could increase the magnitude of bedding parallel contraction resolved on the steepened limbs of pre-existing folds, and thus facilitate development of a second generation of wrench folds upon the earlier folds. Note that other more complicated interpretations for variable orientation of successive fold sets along wrench faults are possible, such as those invoking effects of material anisotropy or stress variations related to tip effects near propagating rupture surfaces (e.g. Pollard & Segall 1987, Sibson 1989).

RELATIONSHIP OF FOLD APPRESSION TO ORIENTATION

Introduction

The trend of hinges of early en échelon folds along the BRFS vary in azimuth between about 045° and 090°, and locally undergo sigmoidal deflections (e.g. Fig. 2). These variations in fold trend suggest that after their nucleation, the early set of wrench folds may have rotated variably clockwise as a result of strain heterogeneity within the BRFS shear zone. The initial orientation of folds in a strike-slip shear zone and the rate of their subsequent rotation and tightening depends on the bulk strain path (Sanderson & Marchini 1984). In addition, the initial orientation of layering and evolving mechanical properties of the buckled multilayer are also important variables. To test the hypothesis of fold rotation and tightening with progressive strain, the acute angle between the strike of the Glacier Creek fault and the strike of the axial surface of adjacent cylindroidal fold segments has been plotted against local fold interlimb angle (Fig. 8a). For each measured fold segment, a mean interlimb angle was determined by eigenvector analysis of planar data from adjoining chevron fold limbs (e.g. Fig. 5, locations E and F). The majority of the data for this analysis were obtained from study of several contiguous F_4 folds in the Valdez Group, which were mapped at their eastern termination against the Glacier Creek fault and traced westward across a wide central domain to a western domain near the axial region of southern Alaska's oroclinal bend (Fig. 2). In the eastern domain, hinges of these folds trend subparallel to the adjacent Glacier Creek fault, but are generally more oblique to that fault as their distance from that structure increases across the central and western domains (Fig. 2) (Little 1990, figs. 7c–e). Of particular interest is the Gravel Creek antiform, which, of the five, was studied in the most detail (Figs. 2 and 5). The axial surface of this fold makes several sigmoidal deflections along its laterally continuous trace (Fig. 2).

Theoretical relationship between interlimb angle and axial plane strike

To help interpret the data, theoretical curves can be constructed describing the variation of axial plane strike with interlimb angle according to different strain paths, such as strike-slip simple shear (Fig. 8c). The construction procedure for these curves assumes that the hinges of ideal chevron-shaped folds (Ramsay 1974) nucleated parallel to λ_1 as resolved on an originally horizontal surface, and that those hinges subsequently behaved either as passive material lines or that the hinges

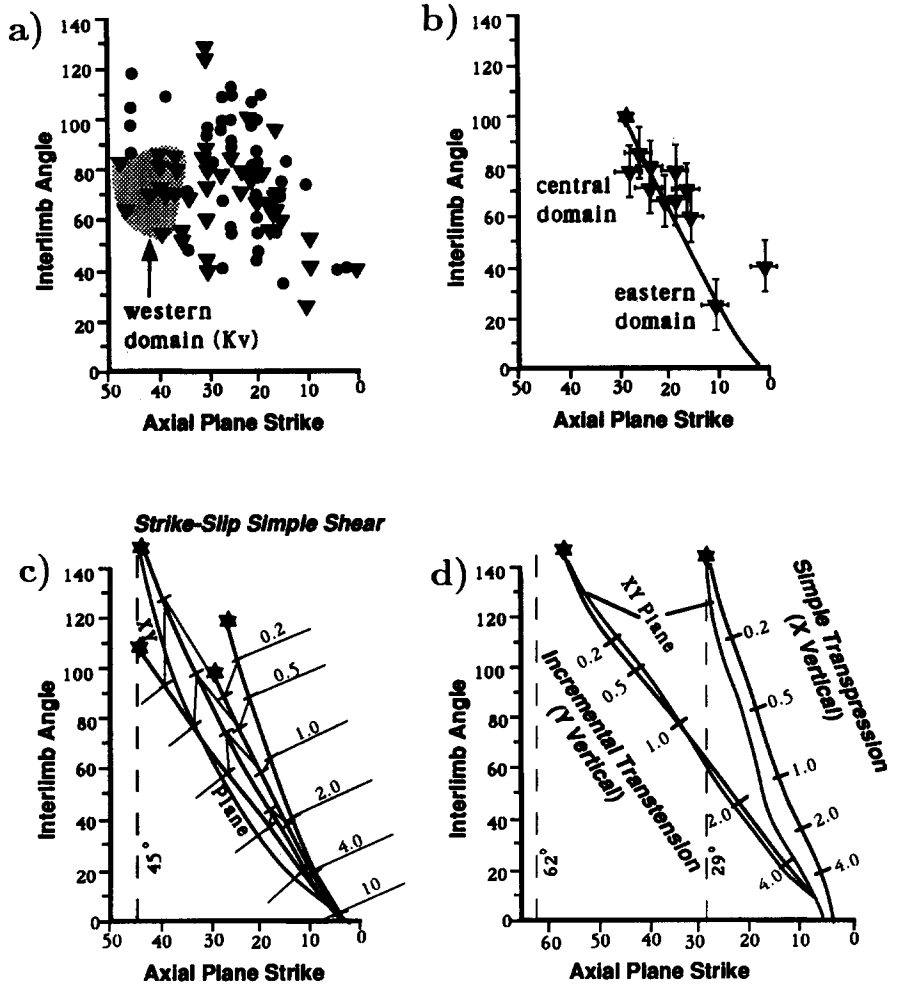

Fig. 8. (a) Interlimb angle vs axial plane strike angle (acute angle with respect to adjacent throughgoing fault) for F_1 folds in the Chickaloon Formation (solid dots); and F_4 folds of the Valdez Group (solid triangles). (b) Subset of above data referring to different segments of the Gravel Creek antiform in the Valdez Group (showing estimated maximum error limits). (c) Theoretical curves for tightening and rotation of selected pre-existing chevron folds by simple shear in a wrench fault zone. Stars denote orientation and interlimb angle of chosen 'initial' folds prior to deformation in the shear zone (i.e. at shear strain, $\gamma = 0$). 'Contours' along curves denote shear strains corresponding to points along the trajectory. Curve labeled 'X–Y plane finite strain' describes trajectory of conceptual chevron folds whose axial planes remain strictly parallel to the X–Y plane of the bulk finite strain ellipsoid (case of hinge migration). (d) Curves as above, but for constant volume 'simple' transpression (right) and a particular path of constant incremental transtension (left). The transtensional path chosen corresponds to the ratio $T_i = \gamma_i(1 - \alpha_i^{-1})^{-1} = -1.33$ (Sanderson & Marchini 1984). Where γ_i is the incremental shear strain parallel to the shear zone boundaries and α_i is the incremental stretch orthogonal to these boundaries (see Fig. 9). This particular value for T_i is consistent with nucleation of late-stage upright folds having axial planes striking at 62° to adjacent throughgoing faults, such as those observed in the BRFS (McCoss 1986).

migrated or 'unrolled' in order to remain parallel to the X–Y plane of the finite strain ellipsoid. Given the angular shape of the folds, the latter assumption seems less likely. For the modeled chevron folds, mechanical layer thickness to wavelength ratios of 0.1–0.01 were chosen, as is consistent with the style of folding in the study area. This analysis is analogous to that of Sanderson (1979), but in this strike-slip setting has the benefit of an *a priori* knowledge of the orientation of the shear zone boundaries. Other curves can be derived from the equations of Sanderson & Marchini (1984), including those for 'simple transpression' and constant incremental transtension (Fig. 8d).

In this analysis we attempt to track the progressive contraction of material lines perpendicular to the axial plane of a pre-existing chevron fold as it is deformed within in a transpressive or transtensive shear zone, and to predict the corresponding change in the interlimb angle of that fold (Fig. 9). The first part of the procedure is to select, *a priori*, the axial plane strike and interlimb angle of the modeled pre-existing fold to be deformed in the shear zone. For the hypothetical case of infinitesimal fold nucleation in a zone of simple shear, one might assign to the fold an original axial plane strike angle, $\beta = 45°$ and an initial interlimb angle of 180°. The initial folds are then strained iteratively by different combinations of shear strain (γ) parallel to the shear zone, and stretch orthogonal to the boundaries, α^{-1} (Fig. 9). Paired values of γ and α corresponding to different points along ideal constant-volume strain paths were chosen from the families of strain paths presented in Sanderson & Marchini (1984). The relationship between

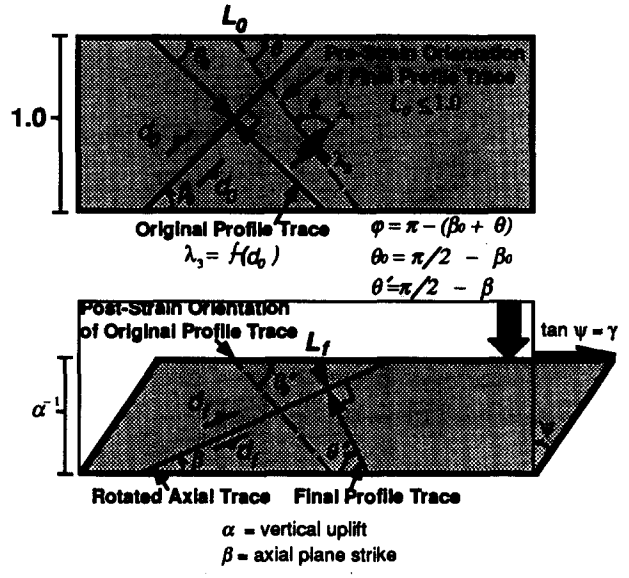

Fig. 9. Geometric model of chevron fold tightening and rotation in a transpressive ductile shear zone (after Sanderson & Marchini 1984). Fold trace prior to deformation (top figure) is parallel to λ_1 of bedding-parallel strain ellipse, makes angle β_0 with respect to shear zone boundary and has limb dips of d_0. Magnitude of λ_3 of strain ellipse is function of d_0. After an increment of shear zone deformation (bottom figure) the fold trace has been rotated to a new angle, β, and the fold limbs now dip at an angle, d_f. Note that fold profile trace after deformation does not coincide with pre-strain profile trace. Material line that will become final fold profile trace originally has a horizontal length of L_0 and the same line after deformation has been additionally shortened to L_f. To preserve volume, a shear zone with a deformed width α^{-1} is stretched in a vertical direction by a factor α.

the original orientation of a material line with respect to the shear zone boundary, θ, and its post-strain orientation, θ', is given by:

$$\cot\theta' = \alpha\cot\theta + \gamma \quad \text{Sanderson \& Marchini (1984).} \tag{1}$$

During the imposed shear zone deformation the increment of reciprocal quadratic elongation, τ'_d, acquired by a horizontal material line that makes an angle, θ', with respect to the shear zone boundary *after* the deformation is given by:

$$\tau'_d = 1 + (\alpha^2 + \gamma^2 - 1)\sin^2\theta' - 2\gamma\sin\theta'\cos\theta' \quad (\textit{ibid.}). \tag{2}$$

This equation can be used to determine the amount of shortening suffered by the line that is oriented normal to the axial plane of the fold after the increment of deformation. The interlimb angle of symmetrical chevron folds as a function of the reciprocal quadratic elongation, τ'_t, of the axial plane normal can be modeled according to the equation:

$$(\tau'_t)^{-1/2} = (1 - \alpha T/L)\cos\left(\frac{\pi-\mu}{2}\right) + T/L\sin\left(\frac{\pi-\mu}{2}\right) \quad \text{Ramsay (1974),} \tag{3}$$

where T is the thickness of the competent members, L is the mean fold limb length, and μ is the fold interlimb angle. For the folds studied T/L is of the order of 0.01–0.1 and a value of 0.05 was used, but use of a different ratio would not affect the analysis significantly. Errors are also introduced by local deviations of the folds from ideal chevron shape.

The total reciprocal quadratic elongation of the post-strain axial plane normal, τ'_t, is the product of that material line's initial elongation, τ'_i (a function of the tightness of the original fold as governed by equation 3), and the additional elongation acquired by the line during the imposed deformation, τ'_d (which leads to further tightening). At the end of a given increment of deformation, the total elongation, τ'_t, of the axial plane normal is:

$$\tau'_t = \tau'_i\tau'_d \quad \text{Sanderson (1979).} \tag{4}$$

Knowing τ'_t, one can solve for the interlimb angle of the strained fold by equation (3). τ'_d is also known from equation (2), thus the only additional information necessary is τ'_i.

This procedure is complicated slightly because different material lines are orthogonal to the axial plane of the fold after each increment of deformation. The initial reciprocal quadratic elongation, τ'_i, of the material line that will later become the axial plane normal is a function of the orientation of this line with respect to the hinge line of the initial fold and the tightness of that initial fold. The initial orientation of this line, θ, with respect to the shear zone boundary can be solved by equation (1), and simple geometry allows us to convert this to an angle, ϕ, of the line with respect to the arbitrarily chosen initial fold hinge line (Fig. 9). Since the initial fold hinge is presumed to lie along the major axis of the bedding plane strain ellipse, we can determine the *initial* reciprocal quadratic elongation, τ'_i, of the line that will later become the fold axial plane normal by:

$$\tau'_i = \tau'_1\cos^2\phi' + \tau'_3\sin^2\phi' \quad \text{Ramsay (1967),} \tag{5}$$

where τ'_1 and τ'_3 are the reciprocal quadratic elongations corresponding to the minor and major axes of the initial bedding-plane ellipse. In practice, τ'_3 was solved by equation (3) by using the arbitrarily chosen interlimb angle of the initial fold, whereas τ'_1 was given extreme values between $1/\tau'_3$ (pure shear) and 1.0 (no axial elongation). The difference in final interlimb angle, β, that resulted from using these two extreme values for τ'_1 in equation (5) was negligible at all except the very highest strains (i.e. β values near zero), where final interlimb angles resulting from the two cases differ by as much as 2°. For these cases the average value was used in Figs. 8(c) & (d).

Results

An admittedly crude relationship of decreasing angle between the strike of fold axial surfaces and the strike of the shear zone boundaries with a corresponding decrease in fold interlimb angle suggests that at least some

early-formed folds were rotated clockwise and tightened by progressive strain within the BRFS (Fig. 8a). Axial surfaces that strike at less than 15° from the shear direction generally have interlimb angles of 30–50° rather than the tight angle predicted by the curves. This observation is probably not surprising given the tendency of chevron folds to lock-up at an interlimb angle about 60° (Ramsay 1967). A different mechanism of layer-parallel shortening may have operated at higher strains, such as reverse faulting (e.g. Fig. 4, B–B′, Fig. 5, location A). In Figs. 8(c) & (d), all the curves have a steep slope connecting an open and obliquely oriented original fold to its tightly appressed, strongly rotated equivalent at very high strains. Thus, without independent strain data the scattered geometric data presented here cannot be used to discriminate between various types of ideal transpressional strain paths. In a general way, however, the data is suggestive of rotation and tightening by some kind of progressive strain involving shortening at a moderate to high angle to the strike of the BRFS.

Sigmoidal deflections in the trace of the Gravel Creek antiform show a fair correlation between axial plane strike and interlimb angle (Fig. 8b). Fold orientation/interlimb angle data from different segments of that undulatory fold suggest local increases in the intensity of shear strain along E-striking dextral shear zones. By considering the Gravel Creek antiform to have had an 'initial' axial surface strike angle of ~30°, and an original interlimb angle of ~100°, superposition of a dextral simple shear strain path could, in a general way, explain the geometry of sigmoidal deflections of the trace of this fold in the central domain. Deflection of the hinge of this fold into an E–W trend adjacent to the Glacier Creek fault is constrained by only two data points, and these suggest a shear strain of at least 3.0 ('eastern domain' data, same figure).

The scattering of data suggests that deformation was heterogeneous, possibly both in time and space. Assuming nucleation of folds at infinitesimal strain, a combination of transpression and simple shear could explain some of the dispersion in the measured data. Local transpression (Fig. 8d) could explain the abundance of close folds with axial planes that strike 15–25° from the shear zone boundary. Note that a transpressive strain path requires a smaller strain (or γ value) to achieve a given amount of rotation than does simple shear or a transtensive path. Other possible explanations for the scattering of fold orientation and interlimb angle data include variations in strain rate or in the stiffness or anisotropy of the folded multilayers, heterogeneities that could result in fold nucleation over a range of threshold stress–strain magnitudes and orientations. In addition, marked variations in the local stress–strain field near a discontinuous rupture surface could result in a wide range of possible initial fold orientations at different locations along the fault surface, or variations at a given location through time as a rupture propagated laterally (e.g. Pollard & Segall 1987). Similarly, variations in friction and magnitude of resolved shear stress on faults could also lead to a range of local stress–strain trajectories and fold orientations.

CONCLUSIONS

In mid Eocene time, distributed ductile wrench deformation along the BRFS resulted in formation of en échelon folds adjacent to active strike-slip faults. These wrench folds deformed an incompletely lithified alluvial fan complex as well as a terrane of underplated phyllitic rocks. Folds in both units are chiefly chevron-shaped and lack an axial planar cleavage. General conclusions arising from this study include the following.

(1) Fold culminations or troughs occur in central parts of sigmoidal folds (possibly situated above concealed strike-slip faults in their basement); or as short segments immediately adjacent to truncating strike-slip faults. Such culminations probably mark zones of increased finite layer-parallel shortening that coincides with sites of fold nucleation, away from which fold tips propagated laterally.

(2) Wrench folding of phyllite at high structural levels was accommodated by flexural-slip between layers up to several meters thick rather than by penetrative flexural-flow along the predominant cleavage.

(3) Arrays of subsidiary faults and syntectonic veins interpreted to have been overprinted on previously strain-hardened folds indicate that fold hinges developed subparallel to the direction of maximum incremental elongation (λ_1), and that incremental λ_2 was vertical.

(4) Although these folds are generally arrayed oblique to the strike of the BRFS, segments of their axial surfaces locally make sigmoidal bends to deflect into subparallelism with adjacent strike-slip faults. The relationship between interlimb angle of the folds and strike of their axial surfaces, although scattered, is consistent with variable clockwise rotation and tightening of at least some of these folds in a zone of heterogeneous, distributed wrench deformation.

(5) Early wrench folds trend clockwise of a younger and generally less tightly appressed fold, a relationship that suggests that the younger folds formed during the same progressive deformational event, but after the earlier set of folds had rotated clockwise, tightened and strain hardened.

(6) Abundant evidence for distributed wrench deformation along the BRFS, and for obliquely disposed principal strain and stress axes suggest that significant frictional shear stresses did accumulate along strike-slip faults in the BRFS, a fault system that is interpreted to have no more than several tens of kilometers of total displacement (Little & Naeser 1989). This situation is unlike that proposed for the modern San Andreas fault by Mount & Suppe (1987), who attribute a lack of obliquely oriented folds along that plate boundary transform fault to weak shear resistance along a narrow, strain-softened fault zone.

(7) Structures in the BRFS also illustrate how strike-slip fault-bend folding can rotate pre-existing wrench

folds within kink band-like domains, and how transtensive deformation, such as that localized within pull-apart grabens, may result in formation of wrench fold hinges that are disposed at a greater than 45° angle with respect to adjacent faults.

Acknowledgements—Field work for this study was made possible by financial support from the State of Alaska, Division of Geological and Geophysical Surveys, and by grants from the Shell Foundation and McGee funds, Stanford University. Additional helicopter support was provided by G. R. Winkler and G. Plafker of the U.S. Geological Survey. Discussions with J. E. Decker, P. B. Gans, J. Lee, E. L. Miller, T. L. Pavlis, G. H. Pessel, G. Plafker, D. D. Pollard and G. R. Winkler stimulated and improved the quality of this research. Criticism by E. L. Miller, two anonymous reviewers, and D. J. Sanderson greatly improved the clarity of the manuscript.

REFERENCES

Angelier, J. 1984. Tectonic analysis of fault-slip sets. *J. geophys. Res.* **89**, 5835–5848.

Aydin, A. & Page, B. M. 1984. Diverse Pliocene–Quaternary tectonics in a transform environment, San Francisco Bay region, California. *Bull. geol. Soc. Am.* **95**, 1303–1317.

Bamford, M. L. F. & Ford, M. 1990. Flexural shear in a periclinal fold from the Irish Variscides. *J. Struct. Geol.* **12**, 59–68.

Bruhn, R. L. & Pavlis, T. L. 1981. Late Cenozoic deformation in the Matanuska Valley, Alaska: three dimensional strain in a forearc region. *Bull. geol. Soc. Am.* **92**, 282–293.

Burns, L. E. 1985. The Border Ranges ultramafic and mafic complex, south-central Alaska: Cumulate fractionates of island arc volcanics. *Can. J. Earth Sci.* **22**, 1020–1038.

Burns, L. E., Little, T. A., Newberry, R. J., Decker, J. E. & Pessel, G. H. 1983. Preliminary geologic map of parts of the Anchorage C-2, C-3, D-2 and D-3 quadrangles, Alaska. *State Alaska Div. geol. geophys. Surv., Rep. Invest.* **83–10**, scale 1:25,000.

Cloos, E. 1955. Experimental analysis of fracture patterns. *Bull. geol. Soc. Am.* **66**, 241–256.

Diblee, T. W. 1977. Strike-slip tectonics of the San Andreas fault and its role in Cenozoic basin evolvement. In: *Late Mesozoic and Cenozoic Sedimentation and Tectonics in California* (edited by Nilson, T. H.). San Joaquin Geological Society, Bakersfield, California, 26–38.

Donath, F. A. & Parker, R. B. 1964. Folds and folding. *Bull. geol. Soc. Am.* **75**, 45–62.

Dubey, A. K. 1980. Model experiments showing simultaneous development of folds and transcurrent faults. *Tectonophysics* **56**, 69–84.

Dubey, A. K. & Cobbold, P. R. 1977. Noncylindrical flexural-slip folds in nature and experiment. *Tectonophysics* **38**, 223–239.

Ghosh, S. K. 1966. Experimental tests of buckling folds in relation to strain ellipsoid in simple shear deformation. *Tectonophysics* **6**, 169–185.

Graham, R. H. 1978. Wrench faults, arcuate fold patterns and deformation in the southern French Alps. *Proc. geol. Ass.* **89**, 125–143.

Harding, T. P. 1974. Petroleum traps associated with wrench faults. *Bull. Am. Ass. Petrol. Geol.* **58**, 1290–1304.

Harding, T. P. 1976. Tectonic significance and hydrocarbon trapping consequences of sequential folding synchronous with San Andreas faulting, San Joaquin Valley, California. *Bull. Am. Ass. Petrol. Geol.* **60**, 356–378.

Harding, T. P. 1988. Comment on "State of stress near the San Andreas fault: Implications for wrench tectonics" (by Mount, V. S. & Suppe, J.). *Geology* **16**, 1151–1152.

Harding, T. P. & Lowell, J. D. 1979. Structural styles, their plate tectonic habitats, and hydrocarbon traps in petroleum provinces. *Bull. Am. Ass. Petrol. Geol.* **63**, 1016–1058.

Harding, T. P., Vierbuchen, R. C. & Christie-Blick, N. 1985. Structural styles, plate tectonic settings and hydrocarbon traps of divergent (transtensional) wrench faults. In: *Strike-slip Deformation, Basin Formation and Sedimentation* (edited by Biddle, K. T. & Christie-Blick, N.). *Spec. Publs Soc. econ. Palaeont. Miner.* **37**, 51–77.

Jones, D. L., Silberling, N. J., Berg, H. C. & Plafker G. 1981. Map showing tectonostratigraphic terranes of Alaska, columnar sections, and summary description of terranes. *U.S. geol. Surv. Open-file Rep.* **81–792**.

Little, T. A. 1988. Tertiary tectonics of the Border Ranges fault system, north-central Chugach Mountains, Alaska: Sedimentation, deformation and uplift along the inboard edge of a subduction complex. Unpublished Ph.D. thesis, Stanford University, California.

Little, T. A. 1990. Kinematics of wrench and divergent-wrench deformation along a central part of the Border Ranges fault system, northern Chugach Mountains, Alaska. *Tectonics* **9**, 585–611.

Little, T. A. & Naeser, C. D. 1989. Tertiary tectonics of the Border Ranges fault system, Chugach Mountains, Alaska: Deformation and Uplift in a forearc setting. *J. geophys. Res.* **94**, 4333–4360.

Little, T. A., Pessel, G. H., Newberry, R. J., Decker, J. E. & Burns, L. R. 1986. Geologic map of parts of the Anchorage C-4, D-4, and C-5 quadrangles, Alaska. *State Alaska Div. geol. geophys. Surv. Publ. Data File Map* **86-28**, scale 1:25,000.

Lonsdale, P. 1988. Paleogene history of the Kula plate: Offshore evidence and onshore implications. *Bull. geol. Soc. Am.* **100**, 733–754.

Magoon, L. B. 1986. Present-day geothermal gradient. In: *Geologic Studies of the Lower Cook Inlet Cost No. 1 Well, Alaska Outer Continental Shelf* (edited by Magoon, L. B.). *Bull. U.S. geol. Surv.* **1596**, 41–46.

McCoss, A. M. 1986. Simple constructions for deformation in transpression/transtension zones. *J. Struct. Geol.* **8**, 715–718.

Michael, A. J. 1984. The determination of stress from slip data: faults and folds. *J. geophys. Res.* **89**, 11,517–11,526.

Moore, J. McM. 1979. Tectonics of the Najd transcurrent fault system, Saudi Arabia. *J. geol. Soc. Lond.* **136**, 441–454.

Mount, V. S. & Suppe, J. 1987. State of stress near the San Andreas fault: Implications for wrench tectonics. *Geology* **15**, 1143–1146.

Nakahara, D. F. & Wiltschko, D. V. 1986. Deformation in the hinge region of a chevron fold, Pennsylvania. *J. Struct. Geol.* **8**, 157–168.

Namson, J. S. & Davis, T. L. 1988. Seismically active fold and thrust belt in the San Joaquin Valley, central California. *Bull. geol. Soc. Am.* **100**, 257–273.

Naylor, M. A., Mandl, G. & Sijpesteijn, C. H. F. 1986. Fault geometries in basement-induced wrench faulting under different initial stress states. *J. Struct. Geol.* **8**, 737–752.

Odonne, F. & Vialon, P. 1983. Analogue models of folds above a wrench fault. *Tectonophysics* **99**, 31–46.

Pavlis, T. L. 1982. Cretaceous deformation along the Border Ranges fault, southern Alaska: Brittle deformation during formation of a convergent margin. *Tectonics* **1**, 343–368.

Pavlis, T. L. 1983. Pre-Cretaceous crystalline rocks of the western Chugach Mountains, Alaska: Nature of the basement of the Jurassic Peninsular terrane. *Bull. geol. Soc. Am.* **94**, 1329–1344.

Plafker, G., Nokleberg, W. J. & Lull, J. J. 1989. Bedrock geology and tectonic evolution of the Wrangellia, Peninsular, and Chugach terranes along the Trans-Alaskan crustal transect in the Chugach Mountains and southern Copper River basin, Alaska. *J. geophys. Res.* **94**, 4255–4295.

Pollard, D. D. & Segall, P. 1987. Theoretical displacements and stresses near fractures in rock: with applications to faults, joints, veins, dikes, and solution surfaces. In: *Fracture Mechanics of Rock* (edited by Atkinson, B. K.). Academic Press, London, 277–349.

Ramsay, J. G. 1967. *Folding and Fracturing of Rock*. McGraw-Hill, San Francisco.

Ramsay, J. G. 1974. Development of chevron folds. *Bull. geol. Soc. Am.* **85**, 1741–1754.

Reches, Z. & Johnson, A. M. 1976. A theory of concentric, kink, and sinusoidal folding and of monoclinal flexuring of compressible elastic multilayers. *Tectonophysics* **35**, 295–334.

Sample, J. C. & Moore, J. C. 1987. Structural style and kinematics of an underplated slate belt, Kodiak and adjacent islands, Alaska. *Bull. geol. Soc. Am.* **99**, 7–20.

Sanderson, D. J. 1979. The transition from upright to recumbent folding in the Variscan belt of southwest England: a model based upon the kinematics of simple shear. *J. Struct. Geol.* **1**, 171–180.

Sanderson, D. J. & Marchini, W. R. D. 1984. Transpression. *J. Struct. Geol.* **6**, 449–458.

Sibson, R. H. 1987. Earthquake rupturing as a mineralizing agent in hydrothermal systems. *Geology* **15**, 701–704.

Sibson, R. H. 1989. Earthquake faulting as a structural process. *J. Struct. Geol.* **11**, 1–14.

Sylvester, A. G. & Smith, R. R. 1976. Tectonic transpression and

basement-controlled deformation in San Andreas fault zone, Salton Trough, California. *Bull. Am. Ass. Petrol. Geol.* **60**, 2081–2102.

Tanner, P. W. G. 1989. The flexural-slip mechanism. *J. Struct. Geol.* **11**, 635–656.

Tanner, W. F. 1961. Surface structural patterns obtained from strike-slip models. *J. Geol.* **70**, 101–107.

Triplehorn, D. M., Turner, D. L. & Naeser, C. W. 1984. Radiometric age of the Chickaloon Formation of south-central Alaska: Location of the Paleocene–Eocene boundary. *Bull. geol. Soc. Am.* **95**, 740–742.

Wickham, J. S. 1988. Comment on "State of stress near the San Andreas fault: Implications for wrench tectonics" (by Mount, V. S. & Suppe, J.). *Geology* **16**, 1152–1153.

Wilcox, R. E., Harding, T. P. & Seely, D. R. 1973. Basic wrench tectonics. *Bull. Am. Ass. Petrol. Geol.* **57**, 74–96.

Winkler, G. R. & Plafker, G. 1981. Geologic map and sections of the Cordova and Middleton Island quadrangles, southern Alaska. *U.S. geol. Surv. Open-file Rep.* **81-1164**.

Wolfe, J. A., Hopkins, D. M. & Leopold, E. B. 1966. Tertiary stratigraphy and paleobotony of the Cook Inlet region, Alaska. *Bull. U.S. geol. Surv.* **1294-A**, A41–A49.

Woodcock, N. H. 1977. Specification of fabric shapes using an eigenvalue method. *Bull. geol. Soc. Am.* **88**, 1231–1236.

Woodcock, N. H. 1986. The role of strike-slip fault systems at plate boundaries. In: *Major Crustal Lineaments and their Influence on Geological History of the Continental Lithosphere* (edited by Reading, H. G., Watterson, J. & White, S. H.). *Phil. Trans. R. Soc. Lond.* **A317**, 13–29.

Woodcock, N. H. & Fischer, M. 1986. Strike-slip duplexes. *J. Struct. Geol.* **8**, 725–735.